

UC Merced

UC Merced Previously Published Works

Title

Real-time identification of the evolution of conducting nano-filaments in TiO₂ thin film ReRAM

Permalink

<https://escholarship.org/uc/item/9c220480>

Journal

Scientific Reports, 3(1)

ISSN

2045-2322

Authors

Song, Seul Ji
Seok, Jun Yeong
Yoon, Jung Ho
et al.

Publication Date

2013

DOI

10.1038/srep03443

Peer reviewed



OPEN

Real-time identification of the evolution of conducting nano-filaments in TiO₂ thin film ReRAM

SUBJECT AREAS:

MATERIALS SCIENCE

MATERIALS FOR DEVICES

Seul Ji Song¹, Jun Yeong Seok¹, Jung Ho Yoon¹, Kyung Min Kim¹, Gun Hwan Kim¹, Min Hwan Lee² & Cheol Seong Hwang¹Received
16 September 2013Accepted
20 November 2013Published
6 December 2013Correspondence and
requests for materials
should be addressed to
C.S.H. (cheolsh@snu.
ac.kr)¹Department of Materials Science and Engineering and Inter-university Semiconductor Research Center, Seoul National University, Seoul, 151-744, Korea, ²School of Engineering, University of California, Merced, 5200 North Lake Rd. Merced, CA 95343, USA.

Unipolar resistance switching (RS) in TiO₂ thin films originates from the repeated formation and rupture of the Magnéli phase conducting filaments through repeated nano-scale phase transitions. By applying the Johnson-Mehl-Avrami (JMA) type kinetic model to the careful analysis on the evolution of transient current in a pulse-switching, it was possible to elucidate the material specific evolution of the Magnéli phase filament. This methodology was applied to the two types of TiO₂ films grown by plasma-enhanced atomic layer deposition (PEALD) and sputtering. These two samples have structurally and electrically distinctive properties: PEALD film exhibited high variability in switching parameters and required an electroforming while sputtered film showed higher uniformity without distinct electroforming process. The JMA-type kinetic analysis of the RS behaviors revealed that the rejuvenation of the filament is accomplished by repeated one-dimensional nucleation followed by a two-dimensional growth in PEALD samples, whereas one-dimensional nucleation-free mechanism dominates in sputtered films.

Dielectric breakdown in metal-insulator-metal (MIM) systems is generally considered to be a catastrophic event for insulating or capacitive applications¹. Recently, the resistance switching (RS) phenomena in several MIM systems has been studied extensively for applications to the next generation non-volatile memory (NVM) devices and memristors^{2–5}. These applications rely on the repeated “controlled soft breakdown” of the insulating films, by electroforming of conducting nano-filaments (CF) and their rupture/rejuvenation. These characteristics make them particularly suitable for next generation NVM devices because potentially it suffers less from the various scaling issues compared to the currently prevailing charge-based memory devices. TiO₂ and NiO are the two of the most extensively studied binary oxide materials for unipolar resistance switching memory devices^{2,3,6–9}. Although RS in NiO, where the CF resembles the dendrite-like structure, has been understood from a random circuit breaker model⁶, the CFs in TiO₂ have been identified as having a distinctive crystalline structure, Magnéli phases (Ti_nO_{2n–1}, where n = typically 4–5), with a conical or cylindrical shape depending on the electroforming condition^{8–11}. Several other RS material systems might have similar distinctive topological phase separation. Kim et al. recently reported that some of the key conclusions from the random circuit breaker model can be derived from the distinctive separated phase CF model by theoretically estimating the generation and dissipation of heat by the flowing current¹¹.

As shown in this report, there are wide variations of RS performances even in devices using the nominally identical TiO₂ materials, which must be closely related with the different configuration and connection/disconnection processes of the CFs in each specific sample. However, the variation cannot be understood from any preexisting models or theories due to the lack of detailed information on the evolution dynamics of the CFs. When the CF has a distinctive phase standing out from the mother insulating phase, such as TiO₂, RS can be considered a local phase transition process. For these cases, preexisting knowledge of the phase transitions, such as the Johnson-Mehl-Avrami (JMA) type kinetic theory^{12,13}, can be used to understand the details of the switching dynamics. Nevertheless, there are two major difficulties when applying JMA theory to the TiO₂ (or any other) RS systems. One is that an accurate estimation of the CF fraction in the mother phase is extremely difficult owing to its extremely tiny dimension and sparse density, which makes a statistically meaningful observation by any microscopic technique almost impossible. The other is the very short time scale (~tens of ns) over which the phase transition occurs. Therefore, observing the transition *in-situ* is generally challenging. *In-situ* transmission electron microscopy (TEM) could not be a viable option for this type of study since TEM can see only a highly



localized area. In addition, the high vacuum environment surrounding the thin foil of TEM specimen is very different from an actual environment of memory device during its operation.

In this study, therefore, the authors developed a new methodology that is accurate and fast enough to estimate the evolution of CFs in a Pt/TiO₂/Pt RS sample by monitoring and modeling the current variation during the switching from off- to on-state when a pulse bias was applied. Current evolution was transformed into the evolution of the volume fraction of the CF, and JMA kinetic theory was applied. The justification for the use of the JMA kinetic model in this seemingly non-isothermal system is given in on-line Supplementary Information (SI). This method may appear simple but the actual implementation requires several precautions, as will be shown in this paper. When this kinetic methodology is applied to two types of TiO₂ films with different crystalline structures, a crucial correlation between the structure and switching parameters was revealed, such as switching voltage, speed, and repeatability. The different deposition method could make the film structure and properties different. The present method, however, can be utilized to understand the kinetic evolution of CFs in any type of switching system as long as the CFs stand out as a distinctive phase from the mother insulating phase.

Results

Resistive switching behaviors depending on the crystal structure.

Two types of Pt/TiO₂/Pt RS cells were fabricated with a 60-nm-thick TiO₂ film, which is grown by either plasma-enhanced atomic layer deposition (PEALD) or RF magnetron reactive sputtering. (See Methods section) Figure 1 shows the crystalline structure and basic RS characteristics of the PEALD and sputtered TiO₂ films. Figure 1 (a) shows the glancing angle X-ray diffraction (GAXRD) patterns of the two films. The PEALD TiO₂ thin film showed only anatase structure, whereas the crystal structure of the sputtered TiO₂ film

is composed of rutile phase. Figures 1 (b) and (c) show the typical unipolar RS current-voltage (I-V) curves of the two films. The unipolar RS process proceeds by applying the same bias polarity for SET (switching from a high resistance state (HRS) to a low resistance state (LRS)) and RESET (switching from LRS to HRS), and was ascribed to the formation (SET) and rupture (RESET) of percolated CFs in transition metal oxides. The most notable difference between the two types of cells is the presence (PEALD TiO₂) and absence (sputtered TiO₂) of an electroforming process. It is expected that this difference would be related to the microstructural and crystallographic differences between the two types of TiO₂ films. This difference may be alternatively understood as follows. The RESET operation of the sputtered sample recovers its pristine state by a 'hard' RESET due to the very high peak RESET current (inset Fig. 1 (b)). This makes the subsequent SET occur at a voltage close to the first SET voltage. The initially slightly leakier property of the sputtered sample compared to the PEALD sample suggests that there are already tiny leakage current paths, which may act as one dimensional nucleus along the film thickness direction for subsequent CF formation during a SET step. The high LRS current implies that there are many CFs formed. However, the occurrence of a hard RESET suggests that each CF is relatively weak, meaning that they recover the pristine state after a RESET. This is related with the columnar grain structure (shown below) and rutile phase of the sputtered film. The leakage paths may have been originally formed along the vertically aligned grain boundaries. This could be understood more evidently from the JMA-type kinetics analysis shown later.

As the Magnéli structure is a rutile-derived structure (The segregation of oxygen vacancies on the (121) planes shear the rutile crystal along the direction in the plane resulting in a Magnéli phase. The total vacancy concentration determines the average distance between the crystallographic shear planes^{14,15}), sputtered TiO₂ films may already contain tiny Magnéli CFs or its embryos in the pristine state. It must be reasonable to assume that crystallographic defects, such as grain boundaries or stacking fault regions in rutile work as the nuclei for Magnéli CFs. On the other hand, the not significantly larger leakage current of the pristine sputtered sample suggests that the density of the possibly built-in CFs in this film is quite low or conductivity of each CF is quite low. In addition, CFs can connect more easily the top and bottom electrodes in the sputtered TiO₂ film because of its columnar structure, whereas PEALD TiO₂ films have a random grain growth structure, as shown by the TEM image in Fig. 2.

Figures 2 (a) and (c) show low magnification bright field TEM images of the PEALD and sputtered sample, respectively, and (b) and (d) are high-resolution TEM images of the squared area shown in (a) and (c). More TEM images of each sample are included in the on-line SI to further confirm the crystal structures. A thin amorphous region (~10 nm) is formed between the crystallized main part of the TiO₂ film and bottom electrode in the sputtered sample probably due to the ionic bombardment effect and possible kinetic mixing with the bottom electrode. The thin interfacial amorphous layer may act as a buffer layer that could improve the switching uniformity. Although extensive TEM investigations were performed, no clear image or diffraction information from the possibly built-in Magnéli phase CFs was achieved from the sputtered sample. This suggests that the embryos of the CF in this sample are extremely small and sparsely distributed, or they do not for the distinctive Magnéli structure yet at the pristine state.

To further understand the difference in the RS properties of the two samples, several RS parameters, such as maximum current of the LRS immediately prior to RESET switching occurs (I_{max}), and the switching time, were estimated and their distributions shown in the insets of Figs. 1 (b) and (c). Here, the switching time was defined as the duration from the moment the voltage is applied to

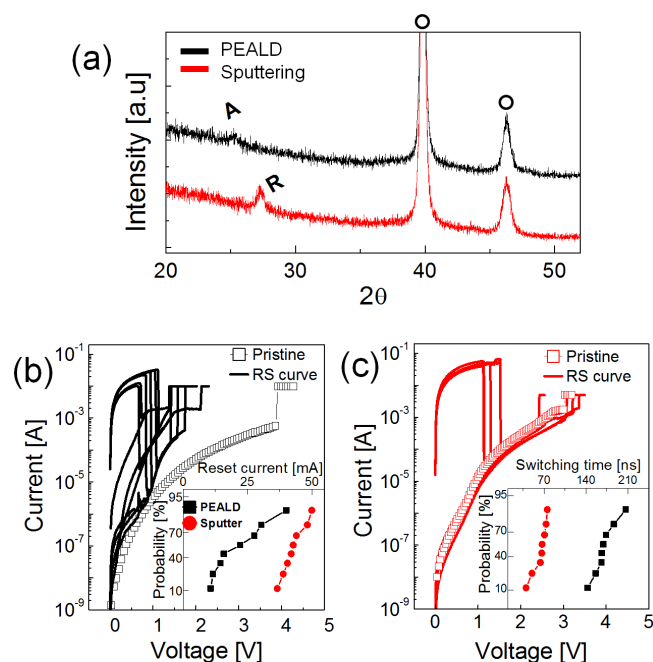


Figure 1 | Crystallographic structure and switching properties of the two samples. (a) GAXRD spectra of the TiO₂ thin films deposited by PEALD (black, upper graph) and sputtering (red, lower graph). PEALD TiO₂ film has an anatase (A) structure, whereas the sputtered TiO₂ film has a rutile (R) structure. The black circles indicate the Pt substrate. (b) and (c) show the typical unipolar resistive switching curves observed in PEALD and sputter-deposited TiO₂ films, respectively. Inset figures in (b) and (c) show the distribution of the switching parameters.

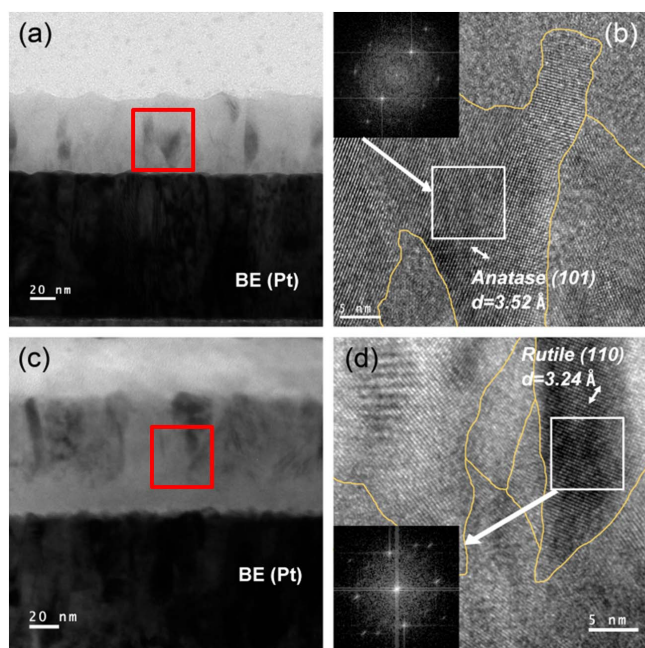


Figure 2 | Microstructure of the prepared TiO₂ films. The cross-section transmission electron microscopy images of (a, b) PEALD and (c, d) sputtered TiO₂ films. The PEALD TiO₂ film has a rather random grain growth structure, whereas the sputtered TiO₂ film shows a more columnar structure on the thin amorphous layer (~10 nm) above the bottom electrode. The thin amorphous layer may act as a buffer layer that promotes rutile phase formation which is not stable phase at the growth temperature (~100°C). HRTEM images correspond to the red square in low magnification images.

the completion of the SET process in pulse switching set-up, which is discussed in detail later. The larger variations in the switching parameters of the HRS in PEALD sample compared to that of sputtered sample are obvious. This suggests that the rupture and rejuvenation of the CF in the sputtered sample was induced repeatedly at the same location, whereas those in the PEALD sample may occur not necessarily at the same location. This is well aligned with the recent report by Yoon et al.^{16,17}. Although set state resistance (R_{SET}) and I_{max} of the two samples are not significantly different, the SET switching time of the sputtered sample is evidently shorter than that of the PEALD sample. This could be ascribed to the structural compatibility between the matrix phase (rutile TiO₂) and Magnéli CF in the sputtered film.

An accurate understanding of the reason why the same bias polarity can induce both SET and RESET switching in unipolar RS is still lacking. Nevertheless, it can be assumed that SET switching is a more electric field-driven phenomenon being thermally assisted by the Joule heating effect because it occurs within a film in HRS over which a significant electric field is applied. On the other hand, a RESET process is understood as a more thermally-activated diffusion process given that the resistance of the CF is generally too low to build a high electric field. Therefore, when the peak current (I_{max}) flowed during the RESET step, the CF must be heated to a temperature possibly high enough to disrupt the ordered structure of the Magnéli CFs and even to (partially) melt them. During the subsequent cooling process, the Magnéli structure may not be recovered sufficiently due to the quenching effect. Recovering the Magnéli structure requires rather extensive diffusion of oxygen vacancies to form the vacancy-ordered structure. The rapid cooling can result in a highly defective TiO_{2-x} through the RESET step. The defect density at this stage can be as high as that of the Magnéli structure or lower than that depending on the detailed nature of the switching process.

In either case, the disordered structure of this material induces a transition to the HRS. During this structural transition, it is highly likely that the phase of neighboring matrix has a significant influence; the quenched material must tend to be anatase- and rutile-like structures in PEALD and sputtered TiO₂ films, respectively, due to the heterogeneous nucleation effect. Subsequent SET switching, therefore, can also be strongly dependent on the structure of the matrix phase. When the quenched region returns to the anatase-like structure in case of the PEALD sample, there may be a relatively low probability that the same region becomes the CF again during the subsequent SET step due to the structural incompatibility between anatase and Magnéli structures, resulting in low repeatability. Therefore, once the CF is ruptured in the PEALD sample, rejuvenation of the CF may require the growth at arbitrary positions among the residual CF fragments during the subsequent SET step. In contrast, the more rutile-like structure of the quenched region in the sputtered TiO₂ can be converted to Magnéli CF more easily by just rearranging the locations of the vacancies inside the material without invoking a structural rearrangement of the entire material. This corresponds to the situation that the one dimensional nuclei of the CF are already present when SET switching begins. These characteristic features of the two types of samples were confirmed experimentally from carefully performed pulse-switching experiments shown below.

Equivalent circuit model for SET transition by a pulse application.

Pulse-switching experiments were performed for both types of samples with a constant current supply using a pulse generator (PG, HP81110A), and the transition current at the moment of SET switching was monitored using a digital oscilloscope (OSC, Tektronix 684C). The PG, sample and OSC are connected in series. (See Methods section and on-line SI for more details^{18,19}.) The equivalent circuit model is included in Fig. 3 (a), and Fig. 3 (b) provides a typical transient current - time evolution when a current pulse was applied to the PEALD sample (data points). The sample was electroformed first and subsequently switched to the RESET state by an I-V sweep before the pulse-switching SET experiment was performed. At the beginning of the pulse application, the sample behaves like an MIM capacitor owing to its high resistance value and capacitor-like structure, and the initial current peak that decays in ~50 ns is due to the completion of capacitive charging. The current increases abruptly between ~150 and ~200 ns corresponding to SET switching, i. e. the ruptured CF is reconnected during that period. Therefore, critical analysis of the transient current in that period can provide information on CF nucleation and growth.

In order to capture the exact time evolution of current that passes through the memory cell during a SET process (the formation of a CF during the sudden current increase at ~150 ns shown in Fig. 3 (b)), the followings factors should be considered. First, when the PG is used as a constant current source, it can be modeled as an ideal current source with its internal resistance (R_{PG}) connected to the sample in parallel. (eq. 1) Second, RS cell becomes a parallel circuit component of the capacitor (C_{mem}) and resistance (R_{mem}) so that the initial capacitor voltage must decay with time, i. e. charge dissipation current (i_{dis}) flows as the CF develops in the sample. The i_{dis} is divided into two components, i_{in} and i_{out} depending on the relative resistance ratio between ($R_{\text{PG}} + R_{\text{OSC}}$) and R_{mem} . (eq. 2) Third, since the R_{mem} is time dependent, the current originating from the PG (i_{leak}) and i_{in} also varies with time. It has been reported that i_{in} has a significant effect on the evolution of R_{mem} ¹⁹⁻²¹. Therefore, an accurate estimation of the actual current flow through R_{mem} [$i_{\text{mem}} (= i_{\text{leak}} + i_{\text{in}})$] requires the establishment of an accurate circuit model and a rather complicated iterative simulation as described in detail below.

Here, C_{mem} was measured to be ~100 pF from low frequency capacitance measurements, and the initial amount of stored charge (q_{mem}) in C_{mem} can be estimated by integrating the charging peak as

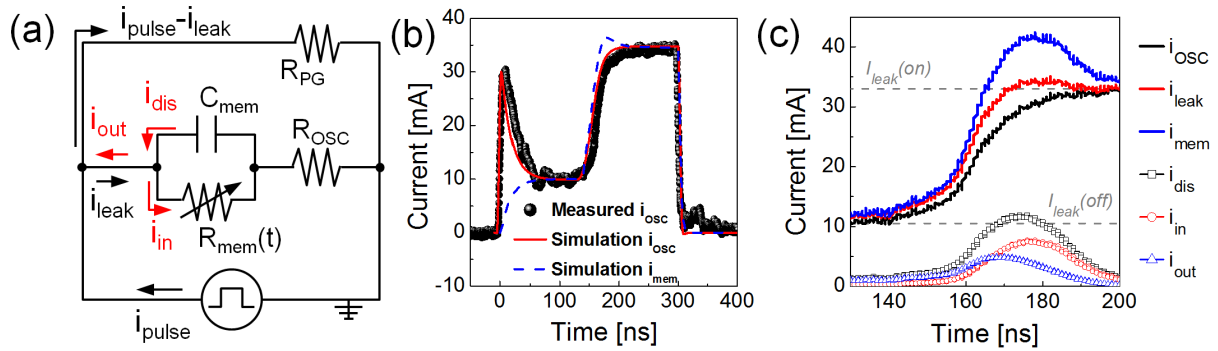


Figure 3 | Pulse-switching experiment for the SET switching of the sample in the RESET state. (a) Schematic diagram of the equivalent circuit model for the pulse switching system, (b) typical SET switching curve with time when a current pulse with 300 ns duration was applied to the device (closed circle). The PSPICE simulation results for the transient current through the OSC (red, line) and memristor device (blue, dash) using an equivalent circuit model. (c) Monitored current (i_{OSC}) and simulated current components (i_{leak} , i_{mem} , i_{dis} , i_{in} and i_{out}) with time.

a function of time. $R_{PG} = R_{OSC} = 50 \Omega$, and a constant current of 80 mA (i_{pulse}) was programmed into the PG for this measurement. The numerical calculation started with the initial conditions of $R_{mem}(t = t_0) = R_{OFF}$ and $i_{dis}(t = t_0) \sim i_{out}(t = t_0) = 0$ and the experimental input values (i_{osc}). The following three equations can be used to evaluate R_{mem} , i_{leak} , etc. as a function of time;

$$\text{Leakage current part : } i_{leak}(t) = i_{pulse} \times \frac{R_{PG}}{R_{PG} + R_{OSC} + R_{mem}(t)} \text{ mA} \quad (1)$$

$$\text{Discharging current part : } \frac{q_{mem}(t)}{C_{mem}} = i_{dis}(t)R_{mem}(t) = \frac{dq_{mem}}{dt} R_{mem}(t) \quad (2)$$

$$i_{out}(t) = i_{dis}(t) \times \frac{R_{mem}(t)}{R_{mem}(t) + R_{PG} + R_{OSC}}$$

$$\text{Monitoring current : } i_{OSC}(t) = i_{leak}(t) + i_{out}(t) \quad (3)$$

First, $R_{mem}(t_0)$ is calculated by substituting $i_{leak}(t_0)$, which is $i_{OSC}(t_0)$, into eq. 1. Subsequently, $i_{dis}(t_0 + \Delta t)$ was found from eq. 2, where dq_{mem}/dt can be approximated as $\{q_{mem}(t_0 + \Delta t) - q_{mem}(t_0)\}/\Delta t = q_{mem}(t_0)/R_{mem}(t_0)C_{mem}$, where Δt is the sampling time of the OSC (0.1 ns). Finally, from the measured value of $i_{OSC}(t_0 + \Delta t)$, $i_{leak}(t_0 + \Delta t)$ can be determined using eq. 3 where the $i_{out}(t_0 + \Delta t)$ was estimated using $i_{dis}(t_0 + \Delta t)$ and eq. 2. At this step, $R_{mem}(t_0 + \Delta t)$ can be calculated from $R_{mem}(t_0 + \Delta t) = 80 \text{ mA } R_{PG}/i_{leak}(t_0 + \Delta t) - (R_{PG} + R_{OSC})$. These steps are repeated until the i_{OSC} is saturated at a certain high level. An example of simulated each current component is shown in Fig. 3 (c) which revealed that the monitored i_{OSC} clearly underestimated the i_{mem} due to the involvement of part of i_{dis} .

Meanwhile, SET switching can be regarded as a local phase transition of the TiO_2 film to the Magnéli phase in the nano-meter scale. Therefore, the equivalent R_{set} is the combined resistance of the Magnéli phase regions (R_{mem}) and the remaining TiO_2 matrix (R_{TiO_2}) in parallel. However, R_{set} can be represented safely as R_{mem} because R_{mem} is much smaller than R_{TiO_2} . To simplify the calculations, the shape of the CFs was assumed to be cylindrical, and the resistivity of the Magnéli phase was assumed to be close to that of the bulk, $\sim 2 \text{ m}\Omega\text{cm}^2$. When R_{mem} was converted to the diameter of the CF, the eventual CF radius was $\sim 70 \text{ nm}$, which is much larger than the previously reported values ($\sim < 10 \text{ nm}$)^{8,9}. This means that the estimated CF diameter corresponds to the sum of several CF formed during this specific SET step, which is discussed in detail below.

Discussion

The time-dependent $i_{leak}(t)$ can be used to estimate the evolution of the volume of CF as a function of time ($\beta_{CF}(t)$) using the following eq. 4;

$$i_{leak}(t) = \frac{V_{mem}(t)}{R_{mem}(t)} = \frac{V_{mem}(t)\beta_{CF}(t)}{\rho d^2}, \quad (4)$$

where d , and ρ is the thickness of the film, and resistivity of Magnéli CF, respectively.

Many of the solid state phase transformations can be regarded as the outcome of two phenomena; nucleation and growth. Under certain circumstances, the well-known JMA theory can be used for an analytical description of their transformation kinetics. In the framework of the JMA theory, the total volume fraction ($X(t)$) of the transformed phase (in this case, Magnéli CF) can be described as eq. 5^{12,13,23–25}.

$$X_i(t) = 1 - \exp(-\kappa t^n) \quad (1 \leq n \leq 4 : \text{Avrami exponent}), \quad (5)$$

where $X_i(t) = \beta_{CF}(t)/\beta_{CF}(\infty)$ which can be assumed to be identical to $i_{leak}(t)/i_{leak}(\infty)$ in this case, and κ is a constant. Detailed justification for the assumption for the replacement of the volume fraction of one- and two-dimensional CF with the current ratio can be found in on-line SI. The JMA theory is based on two general assumptions: 1) there is a constant random nucleation rate, and 2) the growth rate is independent of time throughout the whole volume. These assumptions require constant temperature over time and space. For a given nucleation rate, the JMA kinetic model describes the growth behavior, and the Avrami exponent n is correlated to the dimensional information (D) of the growing phases. When continuous nucleation is accompanied by growth, n becomes $D + 1$, but for retarded nucleation, $n \sim D$. When the TiO_2 sample stays in the HRS, there are large numbers of partial CFs remaining, which might act as nucleation sites for subsequent CF growth. During the subsequent SET switching step, CF growth can occur from any of the remaining partial CFs so the random nucleation hypothesis of JMA model is applicable to this case. Because the tiny size of the CFs ($< \sim 10 \text{ nm}$ in diameter) and the long distance between them make a mutual interaction to be improbable, the first order approximation for the growth kinetics is reasonable. A detailed justification of the application of the JMA model to the RS in these systems can be found in the on-line SI. It is customary to express the JMA equation in the following form;

$$\ln[-\ln\{1-X_i(t)\}] = n \ln t + \ln \kappa, \quad (6)$$

Therefore, the n value for the CF evolution can be achieved by plotting $\ln[-\ln\{1 - i_{leak}(t)/i_{leak}(\infty)\}]$ as a function of $\ln t$.

Figures 4 (a) and (c) show two example plots of $\ln[-\ln\{1 - i_{leak}(t - \tau)/i_{leak}(\infty)\}]$ as a function of $\ln(t - \tau)$ of the PEALD and sputtered TiO_2 films, respectively. τ was introduced to account for the CF incubation time ($\sim 150 \text{ ns}$ for the case of Fig. 3 (b)). The fitting results according to JMA theory show that the JMA model represents the CF formation kinetics well, and interesting variations in the n



value with time are found; n values recur between 1, 2, and 3. There is one notable discrepancy in the variation of n for the two types of samples; for the PEALD TiO_2 case, most of the first n values (10 out of 15 fittings) were 1.04 ± 0.07 , whereas that they were mostly 2.03 ± 0.06 for the sputtered TiO_2 case. Figures 4 (b) and (d) show a histogram of the first exponent for the PEALD and sputtered samples, respectively. This can be understood as follows: for the first n value of 1 (PEALD sample), the second phase (Magnéli CF) is believed to develop initially in one-dimensional mode with the site saturated nucleation. This means that during the previous RESET step, the part of the Magnéli CF in the region near the anode interface ruptures almost completely, and returns to a more anatase-like structure. In the subsequent SET step, the one-dimensional nucleation of a certain CF occurs from the tip of any of the residual CF until it touches the anode (in this case top electrode), whereas nucleation of the other CF is retarded. This must be reasonable because once a certain CF nucleus begins to grow, the field concentration effect further accelerates its growth until it touches the anode, whereas secondary nucleation is retarded during this period. The large variations in the switching parameters shown in Fig. 1 (b), however, suggest that the site for this nucleation is random. The subsequent emergence of n value of 3 in Fig. 4 (a) might correspond to the three-dimensional growth of a given CF, but this is not probable considering the electric field driven nature of CF formation during the SET step. $n = 3$ would be better understood as the two-dimensional thickening of the previously formed one-dimensional nuclei with the simultaneous formation of one-dimensional nuclei growth. The recurrence of $n = 1$ in the third step might correspond to a situation that the growth of all previously formed CF nuclei was complete, and new one-dimensional nuclei growth proceeds.

The absence of $n = 1$ at the first stage in sputtered TiO_2 films coincides with the absence of the electroforming step shown in Fig. 1

(c) and the related discussions above. When RESET was performed previously, a part of the CF near the anode interface must be ruptured, as in the case of a PEALD sample. Nevertheless, it is highly probable that the structure of the resulting insulating phase is rutile-like caused by the influence of the nearby matrix region. Of course, this region must be quite defective. In the subsequent SET step, this defective (previously CF) region may act as the one-dimensional nuclei of CF formation. SET switching begins with a thickening of these already present one-dimensional nuclei without the addition nucleation of one-dimensional nuclei, which corresponds to $n = 2$ of the first stage, as shown in Figs. 4 (c) and (d). Once these preexisting one-dimensional nuclei grow into the large enough CFs, secondary one-dimensional nucleation must occur, which corresponds to the appearance of $n = 1$ in the second stage in Fig. 4 (c). The subsequent emergence of $n = 3$ can be understood similarly as the case of PEALD discussed above. The list of n values for the first and second stages of SET switching for the two samples is included in the on-line SI. From these results, it can be understood that SET switching in this MIM RS system was accomplished by the repeated one-dimensional nucleation and two-dimensional growth of Magnéli CFs until the end of SET operation. Meanwhile, it has to be reminded that R_{mem} for the case of one-dimensional nucleation is not dominated by the resistance of the CF but by that of the region that will be transformed into the CF. However, within the frame work of the one-dimensional nucleation, this does not bring any difference in the analysis results as that region also has a one-dimensional geometry and the same time dependency of the volume change (with opposite sign) of the CF. See on-line SI for more detailed discussions on this aspect.

In conclusion, a general methodology that can be used to deduce the shape and evolution kinetics of CFs in filamentary RS systems is developed by studying transient current response during a SET switching. This method was applied to understand the different

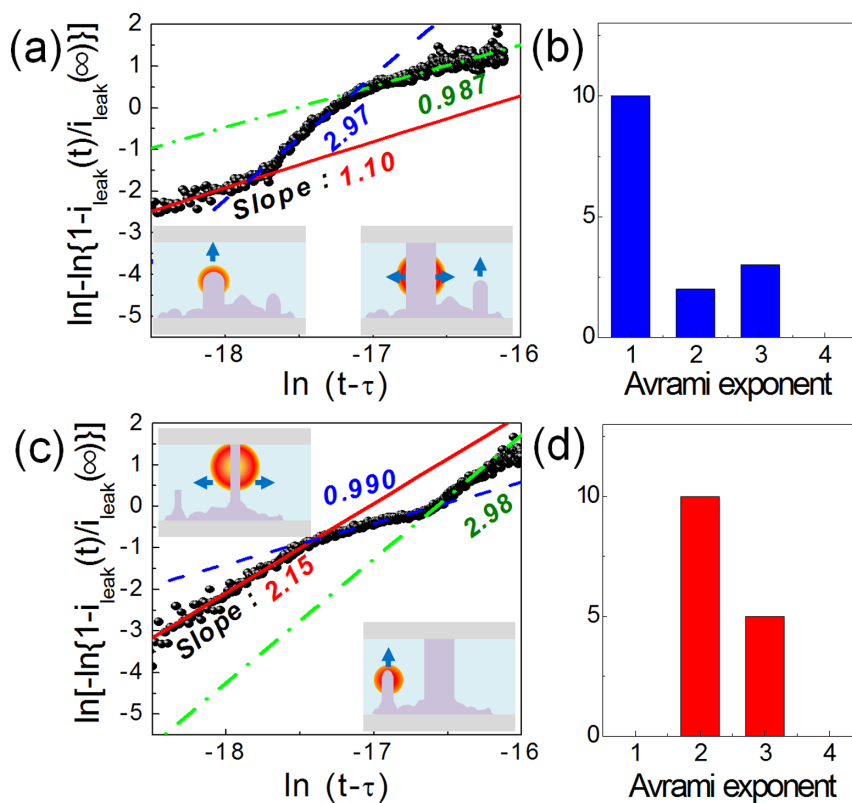


Figure 4 | Comparison of the JMA kinetics fitting results between PEALD and sputtered TiO_2 . (a) and (c) shows the evolution of the reduced leakage current with time for the PEALD and sputtered samples, respectively. The inset figures show schematic diagrams of the CF evolution corresponding to the first and second stages. (b) and (d) shows the distribution of the Avrami exponent of first stages of the PEALD and sputtered samples, respectively.



switching behaviors of two types of TiO₂ RS cells with the same Pt electrodes but different crystallographic and microstructural properties. The difference was induced by different deposition method (PEALD and sputtering). The electrical and physical state of the RESET region in each TiO₂ film was affected largely by the surrounding matrix phase. The rutile structure of the sputtered films appears to help the RESET region retain the same (or a very similar) structure, which facilitates the rejuvenation of the CF during the subsequent SET step at the same location. This is reflected in the better uniformity and repeatability of switching parameters in the sputtered sample compared to the PEALD film. In the PEALD sample, the RESET region may resemble an anatase-like structure, which inevitably induces more random nucleation of the CF during the subsequent SET step. The evolution of the volume fraction of CF with time in the frame of the Johnson-Mehl-Avrami type kinetic model showed that the RESET state of the sputtered sample retains the tiny one-dimensional nuclei of the CF whereas the PEALD sample does not. As a result, the sputtered sample shows SET switching without involving the initial nucleation step, which facilitates fluent and reproducible switching. The PEALD sample requires growth of the one-dimensional CF from the random nucleation sites, which is not necessarily related to previous CF. This kinetic growth model can be applied to other material systems that show filamentary RS characteristics (involving distinct conducting phase CFs), and used as an effective method to determine the geometry of the filaments within these materials. This method also proposes a physical model of the filament growth based on the effect of charge flux through the memory device. This method could find its validity in other unipolar resistance switching system containing Magnéli CFs, such as WO₃, but may be of limited usefulness in other bipolar resistance switching system where no discrete conducting second phases are involved, such as HfO₂ and Ta₂O₅.

Methods

Two types of Pt/60-nm-thick TiO₂/Pt structured samples were fabricated in this study. One type of the samples is a TiO₂ thin film deposited by a plasma-enhanced atomic layer deposition (PEALD) on a sputter-deposited Pt substrate at a growth temperature of 250 °C using Ti(OC₃H₇)₄ as the Ti-precursor and plasma-activated O₂ as the oxygen source¹⁶. The other TiO₂ film was deposited on the same Pt substrate by reactive RF magnetron sputtering using a Ti metal target and 20% O₂ containing Ar gas with a plasma power of 150 W (3 inch diameter of Ti target). After TiO₂ film deposition, a 60 nm-thick platinum electrode was deposited on top of the TiO₂ film by e-beam evaporation using a shadow mask with an electrode area of 60,000 μm² as the top electrode. Such large area samples were most useful for this study because the smaller area samples have an overlap between the initial charging response and the current increase by CF formation. Glancing-angle incidence XRD and TEM were used to characterize the microstructure and crystal structure of the as-grown TiO₂ films. A 200 kV field emission TEM (Tecnai F20) was used for electron diffraction and HRTEM.

The basic resistive switching behavior of the MIM structure samples were measured using an HP4145B semiconductor parameter analyzer in the I-V sweep mode. Pulse switching was performed with a constant current supply using a pulse generator, and the transition current at the moment of SET switching was monitored using a digital oscilloscope. A constant current pulse of 80 mA with a pulse span of 300 ns was programmed to the PG. Since the PG has an internal resistance parallel to the sample, the current flowing through the OSC can be calculated from the relative resistance ratio between the internal resistance of the PG and the total external resistance, which is the sum of the memory and OSC resistance. The measurement system was optimized to prevent the RS characteristics from the interference of signal noise at room temperature. When the parasitic components from the sample itself and circuits were taken into account by the circuit simulation and reference measurement, the time evolution of the total current through the forming CF could be estimated, which was used to estimate the CF growth kinetics using JMA theory.

1. Niemeyer, L. *et al.* Fractal dimension of dielectric breakdown. *Phys. Rev. Lett.* **52**, 1033 (1984).
2. Ahn, S.-E. *et al.* Write current reduction in transition metal oxide based resistance change memory. *Adv. Mater.* **20**, 924 (2008).

3. Strukov, D. B. *et al.* The missing memristor found. *Nature* **453**, 80 (2008).
4. Waser, R. *et al.* Redox-based resistive switching memories—nanoionic mechanisms, prospects, and challenges. *Adv. Mater.* **21**, 2632 (2009).
5. Lee, M.-J. *et al.* A fast, high-endurance and scalable non-volatile memory device made from asymmetric Ta₂O_{5-x}/TaO_{2-x} bilayer structures. *Nature Materials*. **10**, 625 (2011).
6. Lee, J. S. *et al.* Scaling theory for unipolar resistance switching. *Phys. Rev. Lett.*, **105**, 205701 (2010).
7. Yoo, I. K. *et al.* Fractal dimension of conducting paths in nickel Oxide (NiO) thin films during resistance switching. *IEEE Trans. Nanotechnol.* **9**, 131 (2010).
8. Kwon, D.-H. *et al.* Atomic structure of conducting nanofilaments in TiO₂ resistive switching memory. *Nature Nanotechnology*. **5**, 148 (2010).
9. Strachan, J. P. *et al.* Direct identification of the conducting channels in a functioning memristive device. *Adv. Mater.* **22**, 3573 (2010).
10. Kim, K. M. & Hwang, C. S. The conical shape filament growth model in unipolar resistance switching of TiO₂ thin film. *Appl. Phys. Lett.* **94**, 122109 (2009).
11. Kim, K. M. *et al.* Understanding structure-property relationship of resistive switching oxide thin films using a conical filament model. *Appl. Phys. Lett.* **97**, 162912 (2010).
12. Avrami, M. Kinetics of phase change. I. General theory. *J. Chem. Phys.* **7**, 1103 (1939).
13. Avrami, M. Kinetics of phase change. II Transformation-Time relations for random distribution of nuclei. *J. Chem. Phys.* **8**, 212 (1940).
14. Bursill, L. A. & Hyde, B. G. Crystallographic shear in the higher titanium oxides: Structure, texture, mechanisms and thermodynamics. *Progr. Solid State Chem.* **7**, 177 (1972).
15. Liborio, L. & Harrison, N. Thermodynamics of oxygen defective Magnéli phases in rutile: A first-principles study. *Phys. Rev. B*. **77**, 104104 (2008).
16. Yoon, J. H. *et al.* Role of Ru nano-dots embedded in TiO₂ thin films for improving the resistive switching behavior. *Appl. Phys. Lett.* **97**, 232904 (2010).
17. Yoon, J. H. *et al.* Highly improved uniformity in the resistive switching parameters of TiO₂ thin films by inserting Ru nano-dots. *Adv. Mater.* **25**, 1987 (2013).
18. Choi, B. J. *et al.* Study on the resistive switching time of TiO₂ thin films. *Appl. Phys. Lett.* **89**, 012906 (2006).
19. Song, S. J. *et al.* Identification of the controlling parameter for the set-state resistance of a TiO₂ resistive switching cell. *Appl. Phys. Lett.* **96**, 112904 (2010).
20. Kinoshita, K. *et al.* Reduction in the reset current in a resistive random access memory consisting of NiO_x brought about by reducing a parasitic capacitance. *Appl. Phys. Lett.* **93**, 033506 (2008).
21. Ielmini, D. *et al.* Resistance transition in metal oxides induced by electronic threshold switching. *Appl. Phys. Lett.* **94**, 063511 (2009).
22. Acha, C. *et al.* Electrical resistivity of the Ti₄O₇ Magnéli phase under high pressure. *Eur. Phys. J. B* **34**, 421 (2003).
23. Cheng, H.-Y. *et al.* Crystallization kinetics of Ga-Sb-Te films for phase change memory. *Thin Solid Films* **516**, 5513 (2008).
24. Senkader, S. & Wright, C. D. Models for phase-change of Ge₂Sb₂Te₅ in optical and electrical memory devices. *J. Appl. Phys.* **95**, 504 (2004).
25. Allen, J. L. Kinetic study of the electrochemical FePO₄ to LiFePO₄ phase transition. *Chem. Mater.* **19**, 2108 (2007).

Acknowledgments

This study was supported by the Global Research Laboratory program (2012040157) through the National Research Foundation (NRF) of Korea.

Author contributions

S.J.S., J.Y.S. and J.H.Y. performed the sample preparation and electrical measurements. K.M.K., G.H.K. and M.H.L. discussed the technical contexts and made important suggestions. S.J.S. and M.H.L. wrote the parts of manuscript text. C.S.H. conceived the main idea and wrote whole manuscript. All authors reviewed the manuscript.

Additional information

Supplementary information accompanies this paper at <http://www.nature.com/scientificreports>

Competing financial interests: The authors declare no competing financial interests.

How to cite this article: Song, S.J. *et al.* Real-time identification of the evolution of conducting nano-filaments in TiO₂ thin film ReRAM. *Sci. Rep.* **3**, 3443; DOI:10.1038/srep03443 (2013).



This work is licensed under a Creative Commons Attribution-NonCommercial-NoDerivs 3.0 Unported license. To view a copy of this license, visit <http://creativecommons.org/licenses/by-nc-nd/3.0>